Initial-state anisotropies and their uncertainties in ultrarelativistic heavy-ion collisions from the Monte Carlo Glauber model

M. Alvioli,[1,*] H. Holopainen,[2,3,4,†] K. J. Eskola,[2,3,‡] and M. Strikman[5,§]

[1]*ECT, European Centre for Theoretical Studies in Nuclear Physics and Related Areas, Strada delle Tabarelle 286, I-38123 Villazzano (TN) Italy*

[2]*Department of Physics, P.O. Box 35, FI-40014 University of Jyväskylä, Finland*

[3]*Helsinki Institute of Physics, P.O. Box 64, FI-00014 University of Helsinki, Finland*

[4]*Frankfurt Institute for Advanced Studies, Ruth-Moufang-Strasse 1, D-60438 Frankfurt am Main, Germany*

[5]*The Pennsylvania State University, 104 Davey Lab, University Park, Pennsylvania 16803, USA*

In hydrodynamical modeling of heavy-ion collisions, the initial-state spatial anisotropies are translated into momentum anisotropies of the final-state particle distributions. Thus, understanding the origin of the initial-state anisotropies and their uncertainties is important before extracting specific QCD matter properties, such as viscosity, from the experimental data. In this work we review the wounded nucleon approach based on the Monte Carlo Glauber model, charting in particular the uncertainties arising from modeling of the nucleon-nucleon interactions between the colliding nucleon pairs and nucleon-nucleon correlations inside the colliding nuclei. We discuss the differences between the black disk model and a probabilistic profile function approach for the inelastic nucleon-nucleon interactions and investigate the influence of initial-state correlations using state-of-the-art modeling of these.

I. INTRODUCTION

In ultrarelativistic heavy ion collisions performed at Relativistic Heavy Ion Collider (RHIC) and Large Hadron Collider (LHC) elliptic flow—the second Fourier coefficient v_2 that quantifies the azimuthal anisotropy in the measured particle distributions—has been found to be large [1–3]. The appearance of a significant v_2 is a clear signature of pressure formation in the system. It is also consistent with predictions from relativistic hydrodynamics [4,5]: At nonzero impact parameter the overlap area of the colliding nuclei is eccentric in the transverse coordinate plane. This spatial anisotropy is translated first into a flow-velocity anisotropy during the hydrodynamical evolution and, finally, at the decoupling of the system, into a measurable momentum-anisotropy of final-state particle distributions.

Recently it was found out that geometrical fluctuations in the nucleon transverse positions generate initial state anisotropies [6] also for odd harmonics v_n. Nowadays, the experiments at RHIC and LHC have been able to measure nonzero flow coefficients up to v_6 [7–10]. In recent years there have also been considerable developments in event-by-event hydrodynamical modeling [11–16], thanks to which it has become possible to study the higher harmonics [17–19] and v_1 at midrapidity [20–22]. Studies based on hydrodynamics have shown that all initial-state anisotropies are transferred to the final measurable flow values in a similar way as eccentricity is translated to elliptic flow.

In the past few years, much effort has been put on developing viscous hydrodynamics [23–36] and it has turned out that the elliptic flow and especially the higher harmonics are sensitive to the (shear) viscosity η [16,19,37,38]. Since the final flow observables closely reflect the initial-state spatial anisotropies, the uncertainties in the assumed (or computed) initial state are transferred to the computed final-state flow observables. In the studies where one has tried to estimate the shear viscosity-to-entropy ratio, η/s, using elliptic flow measurements, one has seen that the initial eccentricity differences between different initial state models lead to large uncertainties in the extracted value of η/s [27,32]. For determining the shear viscosity from the flow measurements, it is very important to chart all the relevant uncertainties in the computation of the initial asymmetries.

The Glauber model [39] is usually a key element in computing the initial states for hydrodynamical modeling of ultrarelativistic heavy-ion collisions. Some years back, most hydrodynamical calculations assumed smooth initial states where the (energy or entropy) densities were assumed to scale with the density of binary collisions or wounded nucleons computed from the optical Glauber model; see, e.g., Ref. [40]. Now that the importance of the initial density fluctuations has been realized, Monte Carlo Glauber (MCG) modeling has become more frequently used. So far the black disk (hardsphere) modeling of the nucleon-nucleon (NN) interactions has been the standard choice [41–43] in these studies, although also more involved probabilistic ways to model the NN interactions have been known for a long time [39,44–46].

For MCG modeling, one needs the nucleon configurations inside the colliding nuclei as an input for each event. In the simplest approximation the nucleons are assumed point-like and the nucleon positions are obtained by just randomly sampling the Woods-Saxon number density distribution.

*massimiliano.alvioli@pg.infn.it
†holopainen@fias.uni-frankfurt.de
‡kari.eskola@phys.jyu.fi
§strikman@phys.psu.edu

However, to improve the modeling, NN correlations should also be considered, as suggested in Refs. [47–51]. Experimental evidence for the two-body NN correlations generating high-momentum components of the nuclear wave function [52,53], are discussed in Refs. [54–56]. Furthermore, recent studies in Ref. [57] have shown that the effects from including more realistic NN correlations are not negligible, e.g., in the generated initial eccentricity.

In this paper we study for Au-Au collision at RHIC energies, two different uncertainties in computing the initial-state asymmetries from the MCG model: one related to the modeling of the inelastic NN collisions between nucleons from different nuclei, and one related to the NN correlations in the nucleon configurations in each of the colliding nuclei. The paper is organized as follows: In Sec. II A we outline how the initial nucleon configurations can be obtained taking the NN correlations into account. After that, in Sec. II B, we present two different ways to model the inelastic NN primary collisions. The studied initial-state anisotropies are defined in Sec. II C, and results are presented in Sec. III. Finally, the conclusions are drawn in Sec. IV.

II. MONTE CARLO GLAUBER MODEL FRAMEWORK

A. Nucleon configurations

The initial state of a nucleus in the MCG calculations is usually taken as a collection of particles distributed according to a probability distribution given by the corresponding (Woods-Saxon) number density distribution measured in electron scattering experiments. Given the complexity of the nuclear many-body problem, the effects of spatial, spin- and isospin-dependent correlations among the nucleons are usually overlooked and the nucleons are positioned randomly for each of the simulated events.

Recently, in Ref. [47] it was shown how such an approach can be modified by including initial states, which are prepared in advance, in the commonly used computer codes. Also, a method to produce such configurations was introduced. The method is based on the notion of a nuclear wave function ψ, which contains the nucleonic degrees of freedom and which is used to iteratively modify the positions of randomly distributed nucleons using the Metropolis method so that the final positions correspond to the probability density given by $|\psi|^2$. The method is constructed to reproduce the same nucleon number-density distribution as the usual one and, in addition, to reproduce the basic features of the two-nucleon density in the presence of the NN correlations. The model wave function is taken in the form

$$\psi(\boldsymbol{x}_1, ..., \boldsymbol{x}_A) = \prod_{i<j}^{A} \hat{f}_{ij}\, \phi(\boldsymbol{x}_1, ..., \boldsymbol{x}_A), \tag{1}$$

where ϕ is the uncorrelated wave function and $\hat{f}_{ij}$ are correlation operators; here, $\boldsymbol{x}_i$ denotes the position, spin and isospin projection of the ith nucleon. The correlation operator contains a detailed spin-isospin dependence, which is as follows:

$$\begin{aligned}
\hat{f}_{ij} ={}& f^c(r_{ij}) + f^\sigma(r_{ij})\boldsymbol{\sigma}_i \cdot \boldsymbol{\sigma}_j + f^\tau(r_{ij})\boldsymbol{\tau}_i \cdot \boldsymbol{\tau}_j \\
& + f^{\sigma\tau}(r_{ij})\boldsymbol{\sigma}_i \cdot \boldsymbol{\sigma}_j \boldsymbol{\tau}_i \cdot \boldsymbol{\tau}_j + f^t(r_{ij})\hat{\boldsymbol{S}}_{ij} \\
& + f^{t\tau}(r_{ij})\hat{\boldsymbol{S}}_{ij}\boldsymbol{\tau}_i \cdot \boldsymbol{\tau}_j + \cdots,
\end{aligned} \tag{2}$$

where r_{ij} is the relative distance between nucleons i and j, $\boldsymbol{\sigma}_i$ and $\boldsymbol{\tau}_i$ are the Pauli spin and isospin operators, respectively, and $\hat{\boldsymbol{S}}_{ij}$ is the so-called tensor operator (see, e.g., Ref. [52]), which depends on the spin and spatial variables of nucleons i and j. In the most general case, the sum extends over a number of channels that are the same as the one appearing in modern nucleon-nucleon potentials used to successfully describe a variety of properties of light and medium-heavy nuclei within different *ab initio* approaches. When all the correlation functions in Eq. (2), except the first one [$f^c(r)$], vanish, we have the central correlation case.

In this paper we will consider configurations produced both with the central correlations only (denoted in the following by *central*) and with a full set of the six correlation functions of Eq. (2) (denoted by *full*), including the tensor operator. These correlation functions [52] were developed by variational method for nuclei lighter than ^{197}Au considered in this paper; nevertheless, they represent the best approximation that we can offer, since no corresponding calculations exist for heavy nuclei. More specifically, we used correlation functions obtained for ^{40}Ca. Many recent theoretical works support the universality of NN correlations in nuclei [58–60]. We justify the use of ^{40}Ca correlation functions by the observation that they differ very little from those obtained for ^{16}O; ^{40}Ca is a large enough nucleus to neglect additional differences with ^{197}Au due to A dependence in this context, as well as differences arising from the fact that correlation functions were obtained for doubly magic, symmetric nuclei such as ^{16}O and ^{40}Ca. Moreover, as shown in Ref. [48], the two-body densities resulting from configurations obtained using these correlations are clearly more realistic than the completely uncorrelated ones.

The method developed in Ref. [47] allows in principle to deal with any set of correlations; nevertheless, although the state-dependent correlations introduce an extra computational effort due to their noncommutative nature, they can be treated up to a certain degree. In this paper we have used configurations including two-body full correlations, and configurations of three-body clusters surrounding each of the nucleons, induced by full correlations. Genuine three-body correlations will also be discussed in the following.

B. Modeling the inelastic interactions

We work in the Glauber model framework [39], neglecting the effects of inelastic diffraction that lead to fluctuations of the strength of the NN interactions [61,62]. To generate the inelastic NN collisions of interest here, we use the following two different approximations for deciding whether a collision between the nucleons i and j from different nuclei takes place:

(i) *Black disk* approximation, used recently, e.g., in Ref. [15], where one assumes the two nucleons to interact inelastically with a probability one if their

transverse separation b_{ij} is within a radius defined by the inelastic NN cross section $\sigma_{NN}^{\rm in}$,

$$b_{ij}^2 \leqslant \frac{\sigma_{NN}^{\rm in}}{\pi}; \qquad (3)$$

(ii) *Profile function approach*, where the probability of an inelastic interaction between the nucleons i and j is given by

$$P(\boldsymbol{b}_{ij}) = 1 - |1 - \Gamma(\boldsymbol{b}_{ij})|^2, \qquad (4)$$

and where the profile function Γ is expressed in terms of the total and elastic NN cross sections as follows:

$$\Gamma(\boldsymbol{b}_{ij}) = \frac{\sigma_{NN}^{\rm tot}}{4\pi B} e^{-b_{ij}^2/(2\,B)}, \qquad (5)$$

with $B = (\sigma_{NN}^{\rm tot})^2/(16\pi \sigma_{NN}^{el})$.

The probability distribution $P(\boldsymbol{b}_{ij})$ can be derived in the Born approximation of the potential-scattering formalism, by parametrizing the NN elastic scattering amplitude as [39,49,61]

$$f(\boldsymbol{q}) = \frac{C(i + \alpha)k}{4\pi} e^{-\frac{1}{2}Bq^2}, \qquad (6)$$

where C and B are constants to be determined, $k \approx E$ and $\alpha \approx 0$ for ultrarelativistic energies. For the small-angle scatterings of interest here, the vector **q** corresponds to the difference between the incoming and scattered wave vectors in the transverse plane, and $q = |\boldsymbol{q}|$ relates to the scattering angle as $q \approx k\theta$. We fix C to the measured $\sigma_{NN}^{\rm tot}$ on the basis of the optical theorem,

$$\sigma_{NN}^{\rm tot} = \frac{4\pi}{k} Im[f(\boldsymbol{0})]. \qquad (7)$$

The profile function in Eq. (5) is obtained as a Fourier transform,

$$\Gamma(\boldsymbol{b}_{ij}) = \frac{1}{2\pi i k} \int d^2\boldsymbol{q}\, e^{-i\,\boldsymbol{q}\cdot\boldsymbol{b}_{ij}}\, f(\boldsymbol{q}), \qquad (8)$$

and the elastic NN cross section from this as

$$\sigma_{NN}^{\rm el} = \int d^2\boldsymbol{b}_{ij}\, |\Gamma(\boldsymbol{b}_{ij})|^2. \qquad (9)$$

Thus, we have

$$\sigma_{NN}^{\rm el} = \frac{(\sigma_{NN}^{\rm tot})^2}{16\pi B}, \qquad (10)$$

$$\sigma_{NN}^{\rm tot} = \sigma_{NN}^{\rm el} + \sigma_{NN}^{\rm in}, \qquad (11)$$

and B can be fixed on the basis of measured cross sections. For the current setup at $\sqrt{s_{NN}} = 200$ GeV, we take $B = 14$ GeV^{-2} and $\sigma_{NN}^{\rm tot} = 52$ mb, which correspond to $\sigma_{NN}^{\rm in} = 42$ mb and $\sigma_{NN}^{\rm el} = 9.9$ mb.

Finally, using Eqs. (7), (9), and (11), we arrive at the probability function of Eq. (4), whose integral over the transverse separation gives the inelastic NN cross section:

$$\sigma_{NN}^{\rm in} = \int d^2\boldsymbol{b}_{ij}\, [2\,Re\,\Gamma(\boldsymbol{b}_{ij}) - |\Gamma(\boldsymbol{b}_{ij})|^2]$$

$$= \int d^2\boldsymbol{b}_{ij}\, [1 - |1 - \Gamma(\boldsymbol{b}_{ij})|^2]. \qquad (12)$$

C. Spatial asymmetries and their fluctuations

In this section we define the initial state anisotropies, which are studied in this work. We focus on the first three harmonics $n = 1, 2, 3$: dipole asymmetry, eccentricity, and triangularity. Higher harmonics are left out since they are more complicated due to the fact that they can be mainly originating from the lower harmonics [63]. Also, from the experimental results we know that the second and third harmonics are the largest ones.

We calculate the asymmetries from the wounded nucleon positions which are obtained from the MCG model. In the following, the angle brackets denote an average over wounded, or participant, nucleons. The asymmetries are defined as

$$\epsilon_n = -\frac{\langle w(r)\cos[n(\phi - \psi_n)]\rangle}{\langle w(r)\rangle}, \qquad (13)$$

where $w(r)$ is a weight and ψ_n is an orientation angle that is obtained as

$$\psi_n = \frac{1}{n}\arctan\frac{\langle w(r)\sin(n\phi)\rangle}{\langle w(r)\cos(n\phi)\rangle} + \frac{\pi}{n}, \qquad (14)$$

where arctan is always placed in the correct quadrant. These quantities are always calculated in the center-of-mass of the wounded nucleon system. We choose to use $w(r) = r^3$ for $n = 1$, $w(r) = r^2$ for $n = 2$, and $w(r) = r^3$ for $n = 3$ [20].

We also study the fluctuations of the initial-state asymmetries since the current flow analysis methods are sensitive to the fluctuations of the flow coefficients [64]. Since final flow values reflect the initial-state asymmetries, the fluctuations of the flow coefficients should follow the initial-state fluctuations. We define the fluctuations of the anisotropies as

$$\Delta\epsilon_n = \sqrt{\frac{\sum(\epsilon_n^i - \langle\epsilon_n\rangle)^2}{N}}, \qquad (15)$$

where ϵ_{n^i} is the asymmetry in event i and $\langle\epsilon_n\rangle$ denotes the average over N events.

III. RESULTS

A. Number of wounded nucleons and binary collisions

First we look how the interaction models and NN correlations affect the number of the participants ($N_{\rm part}$) and binary collisions ($N_{\rm coll}$). In Fig. 1 we have plotted these as a function of the impact parameter. One can see that in central collisions the results are the same with both interaction models, but when impact parameter becomes large, $b = 10 - 15$ fm, i.e., when only the edges of the nuclei collide and when the number of participants and binary collisions are of the same order, the difference between models is over 5%. This holds both for wounded nucleons and binary collisions. From Fig. 1 it can be seen that the effects of NN correlations on these quantities are very small.

B. Effects of the interaction model on ϵ_n and their fluctuations

Next, we consider the two different interaction models discussed in Sec. II B and present their effects on the anisotropies defined above. In these calculations the NN correlations are
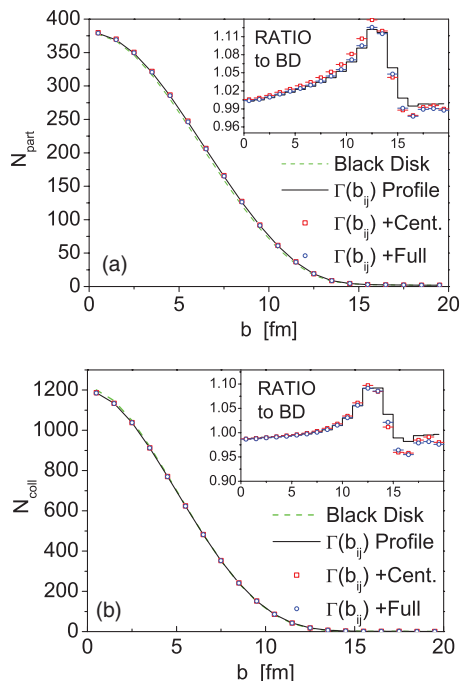
FIG. 1. (Color online) Number of wounded nucleons (a) and binary collisions (b) as a function of impact parameter with different interaction models and initial-state configurations. The results shown correspond to the black disk approximation with uncorrelated configurations (green dashed line); the profile function approach $\Gamma(b_{ij})$ with uncorrelated configurations (black solid line); the profile function approach with central NN correlations (red squares); and the profile function approach with full NN configurations (blue circles). The insets show the ratios of the last three cases to the black disk + uncorrelated one, with corresponding notations.

neglected for clarity; the effects of these correlations will be studied in the next section. In Fig. 2 we have plotted the anisotropies ϵ_1, ϵ_2, and ϵ_3 as a function of N_{part} using the black disk and profile function approaches to model the inelastic NN collisions. The black disk approximation results in larger dipole asymmetry ϵ_1, eccentricity ϵ_2, and triangularity ϵ_3. In all cases, the obtained asymmetries in the profile function approach are slightly ($\lesssim 10\%$) smaller than in those in the black disk case. Apparently, toward peripheral collisions, we have more fluctuations and a less-well-defined shape with the profile function approach, hence a smaller ϵ_n.

The difference between these two cases is negligible in most central collisions for every n. When moving toward peripheral collisions, the results start to deviate from each other and the largest difference is approximately on the order of 10%. In central collisions, most of the nucleons experience several collisions and, thus, the details of the collision model are not very important. In peripheral collisions, however, more and more of the nucleons collide only once or twice, meaning that the interaction model details start to play a role. One must also remember that as we saw from Fig. 1, the events with the same impact parameter are mapped to slightly smaller N_{part} values with the black disk interaction model.

In Fig. 3 we plot the relative fluctuations of the initial-state anisotropies. Here the order of the curves is opposite compared
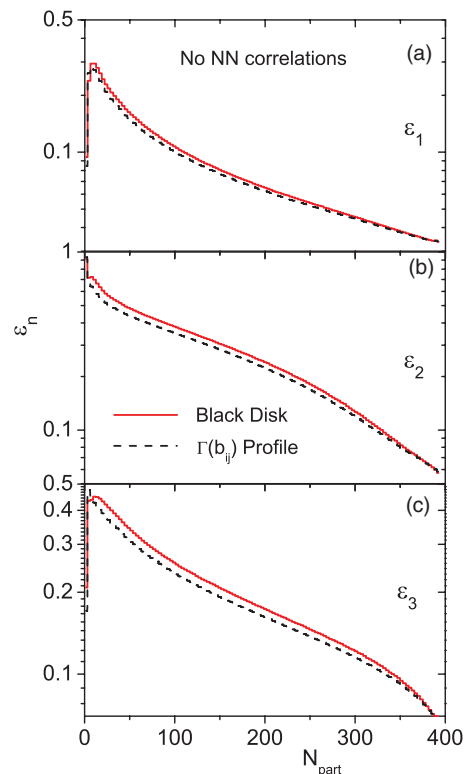

FIG. 2. (Color online) First three harmonics ϵ_n as a function of the number of participants. Results shown are for the two different interaction models. In these plots no NN correlations are taken into account.

to the ϵ_n when $n = 2, 3$. This means that at least partly the difference in the relative fluctuations is explained simply by the fact that the absolute value is slightly higher in the case where the relative fluctuations are smaller. For ϵ_1 the relative fluctuations are larger with black disk interaction, indicating that then also the absolute fluctuations are larger with black disk than profile interaction.

The relative fluctuations of ϵ_1 show a decreasing trend when approaching central collisions but the impact-parameter dependence is relatively weak. On the other hand, the relative fluctuations of ϵ_2 clearly depend on the impact parameter. In central collisions the fluctuations are large, since the system is azimuthally very symmetric, and toward peripheral collisions the fluctuations decrease, since the collision area becomes clearly eccentric. Triangularity ϵ_3 has yet another behavior: its relative fluctuations stay approximately constant when $N_{\text{part}} > 100$. Since the triangularity is created purely by the fluctuations in the positions of wounded nucleons, we can expect that the relative fluctuations have no centrality dependence. All in all, $\Delta\epsilon_1/\epsilon_1$ and $\Delta\epsilon_3/\epsilon_3$ have only a mild centrality dependence, while $\Delta\epsilon_2/\epsilon_2$ exhibits a clear dependence on the centrality. In addition, we conclude that for these relative fluctuations, the NN interaction model uncertainties do not play a major role.

C. Effects of the NN correlations on ϵ_n and their fluctuations

Next, we investigate the effects of different models for the initial state NN correlations. We have chosen to use the $\Gamma(b_{ij})$
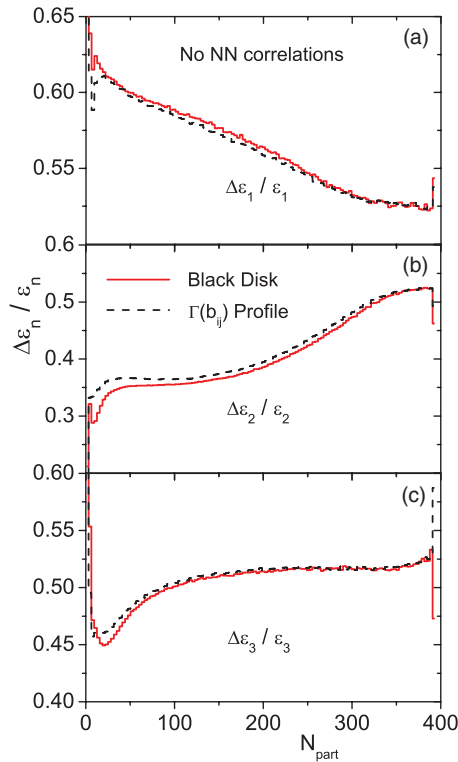
FIG. 3. (Color online) Relative fluctuations of the first three harmonics ϵ_n as a function of number of participants. Results are shown with two different interaction models. In these plots, no NN correlations are taken into account.

FIG. 4. (Color online) First three harmonics ϵ_n as a function of number of participants. Results are shown with different NN correlations and using the $\Gamma(b_{ij})$ collision profile function approach.

collision profile function in these calculations. In Fig. 4 we have plotted the obtained anisotropies with three different NN correlations: no correlations at all, only central correlations and full correlations. From all panels we see that no correlations and full correlations are very close to each other, but the central correlations have a smaller anisotropy.

In all cases the difference between central correlations and the two other cases is largest at central collisions and it gets smaller toward peripheral collision. Nucleon correlations are most important in the middle of the nucleus since the nucleon density is largest there. Thus, in the central collisions, where most of the wounded nucleons come from the middle of the nuclei, the effect on anisotropies is largest. When moving toward the peripheral collisions, the relative amount of wounded nucleons coming from the edges of nuclei is increasing. Thus, in very peripheral collisions where only the edges are overlapping, the effect disappears.

We must bear in mind that central correlations have only repulsive character; their effect can be mimicked by an ad-hoc exclusion radius, as shown in Ref. [57]. Full state-dependent correlations, instead, have a complex structure, which causes nucleons to be at a given average distance in the nucleus and results in nuclear binding and its saturation with increasing A. Partially including these full correlations and disregarding three-body repulsion, as it is explained below, produces the net result of working in the opposite direction of repulsion, for the considered quantities.
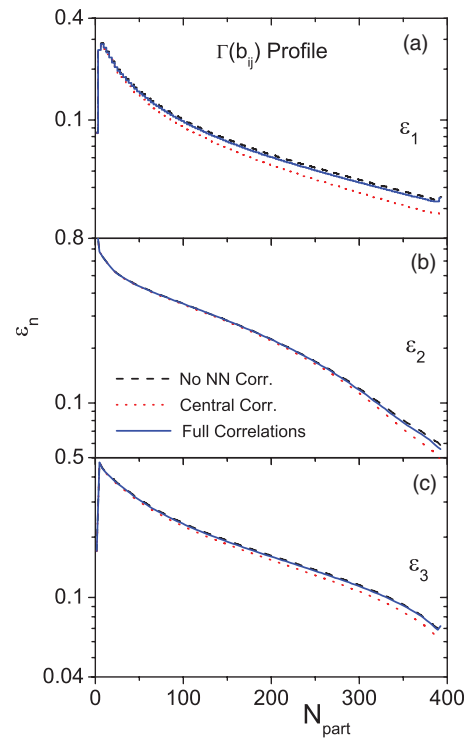
Next, in Fig. 5, we plot the relative fluctuations of anisotropies with different initial state NN correlations. We can see that inclusion of full correlations brings the results back toward the uncorrelated case; this is less evident for $\Delta\epsilon_3/\epsilon_3$. However, now the difference is small in the central collisions and it is largest in the semiperipheral collisions. The difference again vanishes at the most peripheral collisions.

The results obtained with realistic configurations deserve some discussion. The production of configurations with full realistic correlation functions differs substantially from the central correlations case, since in the realistic description there are several spatially dependent correlation functions complemented with spin- and isospin-dependent operators, as shown in Eq. (2). At this stage, we have performed a truncation of the chains induced by realistic correlations at the level of three-particle chains; in principle, due to the noncommutativity of the operators in Eq. (2), the chains are A-body operators. Moreover, we restricted our calculations to three particles which are within a given radius from the active particle in the Metropolis algorithm. It should be stressed that these kinds of simplifications are not suggested by specific physics arguments but are rather dictated by the enormously increasing computing time. As a result, the truncation obviously induces some amount of uncertainty in our results. The overall trend, that the full correlations seem to bring the results back toward the no correlation case, is nevertheless what we wish to emphasize here.

In order to illustrate the effect of the truncation, we have repeated the calculation with configurations including only two-body, realistically correlated clusters (2b only), and
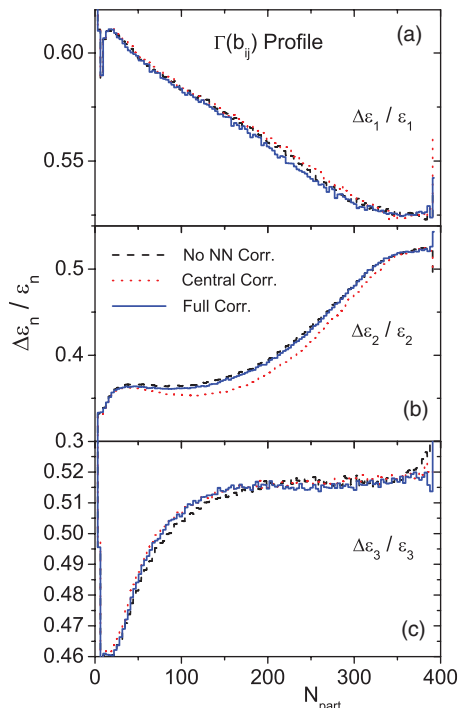
of two-body state-dependent correlations and to the genuine three-body correlations, which we have not included here. The outcome of such a study is, however, difficult to predict, due to the complicated interplay of attraction and repulsion between the three particles in different spin and isospin states.

IV. CONCLUSIONS

In this paper we have charted some of the uncertainties in the computation of the initial state anisotropies from the Monte Carlo Glauber model. We used two different ways of modeling the inelastic interactions between the colliding nucleons. The difference between these two cases gives us an estimate about the uncertainties related to this part of the model: in central collisions the details of the interaction model play a minor role, but in the peripheral collisions such details can cause uncertainties up to 10% in the first three harmonics, ϵ_1, ϵ_2, and ϵ_3. We also checked that with these two interaction models the difference in the number of wounded nucleons and binary collisions remains small in central collisions, but at impact parameters 10–15 fm the difference can be around 10%. We also note that during the writing process of this article, a similar nucleon interaction model study was released in Ref. [65]. The main differences to our study are the different form of the elastic NN scattering amplitude as well as the treatment of the NN correlations.

We also presented a study of the effects of NN correlations with an update of correlated configurations and extended discussion as compared with the previous published papers on this subject. We confirmed that the inclusion of centrally correlated nucleon configurations produce the effects to eccentricity and its relative variance as was claimed by Ref. [57]. As a new result, we observed that the inclusion of realistically correlated configurations (two-body full correlations, three-body chains) seems to essentially cancel this effect and bring the results back close to the no correlations case. The effect is similar for dipole asymmetry and triangularity as for eccentricity. However, we also showed that there are still uncertainties caused by the truncation done in the nucleon configuration calculation with full correlations and we expect three-body correlations to play a role.

In this paper we studied two sources of additional uncertainty in the Monte Carlo model calculations for the initial-state anisotropies. The uncertainty caused by the studied effects to these anisotropies was found to be maximally of the order of 10%. Now that—thanks to the recent developments in event-by-event hydrodynamics—more precise comparisons of flow coefficients between the data and the theory are becoming possible, it is important to chart all the relevant uncertainties to this precision, so that the QCD matter properties could eventually be determined from the measured particle spectra and their azimuthal asymmetries.

FIG. 5. (Color online) Relative fluctuations of the first three harmonics ϵ_n as a function of the number of participants. Results are shown with different NN correlations and using the $\Gamma(b_{ij})$ collision profile approach.

compared with the three-body calculation outlined above (3b chains). The results for $\Delta\epsilon_2/\epsilon_2$ are compared with the corresponding uncorrelated and central correlation case in Fig. 6. Interestingly, it can be seen that the full correlations with the 2b chains cause an effect into the opposite direction than the more advanced 3b chains do. Although beyond the scope of this paper, it would be interesting to study how sensitive the considered anisotropies, and also the higher moments of participant matter distribution, are to the higher-order chains
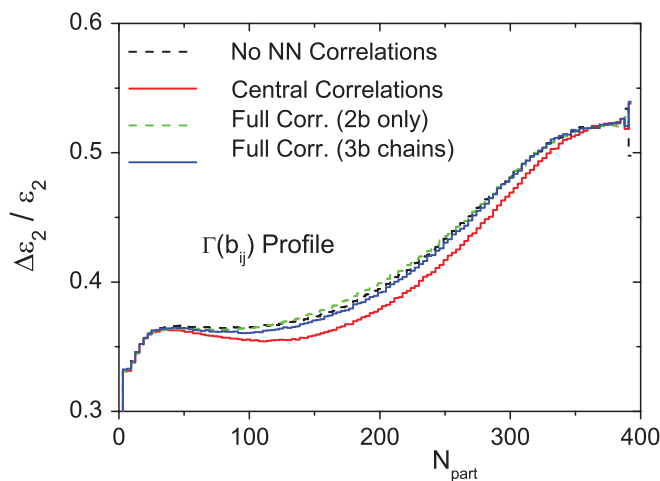

FIG. 6. (Color online) The effect of different models of realistic correlations on the relative fluctuations of eccentricity; see text for explanation.

[1] K. H. Ackermann *et al.* (STAR Collaboration), Phys. Rev. Lett. **86**, 402 (2001).

[2] K. Adcox *et al.* (PHENIX Collaboration), Phys. Rev. Lett. **89**, 212301 (2002).

[3] K. Aamodt *et al.* (ALICE Collaboration), Phys. Rev. Lett. **105**, 252302 (2010).

[4] P. Huovinen, P. F. Kolb, U. W. Heinz, P. V. Ruuskanen, and S. A. Voloshin, Phys. Lett. B **503**, 58 (2001).

[5] J.-Y. Ollitrault, Phys. Rev. D **46**, 229 (1992).

[6] B. Alver and G. Roland, Phys. Rev. C **81**, 054905 (2010).

[7] A. Adare *et al.* (PHENIX Collaboration), arXiv:1105.3928 [nucl-ex].

[8] P. Sorensen (STAR Collaboration), J. Phys. G **38**, 124029 (2011).

[9] K. Aamodt *et al.* (ALICE Collaboration), Phys. Rev. Lett. **107**, 032301 (2011).

[10] J. Jia, J. Phys. G **38**, 124012 (2011).

[11] R. Andrade, F. Grassi, Y. Hama, T. Kodama, and O. Socolowski Jr., Phys. Rev. Lett. **97**, 202302 (2006).

[12] R. P. G. Andrade, F. Grassi, Y. Hama, T. Kodama, and W. L. Qian, Phys. Rev. Lett. **101**, 112301 (2008).

[13] H. Petersen and M. Bleicher, Phys. Rev. C **79**, 054904 (2009).

[14] K. Werner, I. Karpenko, T. Pierog, M. Bleicher, and K. Mikhailov, Phys. Rev. C **82**, 044904 (2010).

[15] H. Holopainen, H. Niemi, and K. J. Eskola, Phys. Rev. C **83**, 034901 (2011).

[16] B. Schenke, S. Jeon, and C. Gale, Phys. Rev. Lett. **106**, 042301 (2011).

[17] G.-Y. Qin, H. Petersen, S. A. Bass, and B. Muller, Phys. Rev. C **82**, 064903 (2010).

[18] Z. Qiu and U. W. Heinz, Phys. Rev. C **84**, 024911 (2011).

[19] B. Schenke, S. Jeon, and C. Gale, Phys. Rev. C **85**, 024901 (2012).

[20] D. Teaney and L. Yan, Phys. Rev. C **83**, 064904 (2011).

[21] M. Luzum and J.-Y. Ollitrault, Phys. Rev. Lett. **106**, 102301 (2011).

[22] F. G. Gardim, F. Grassi, Y. Hama, M. Luzum, and J.-Y. Ollitrault, Phys. Rev. C **83**, 064901 (2011).

[23] P. Romatschke and U. Romatschke, Phys. Rev. Lett. **99**, 172301 (2007).

[24] K. Dusling and D. Teaney, Phys. Rev. C **77**, 034905 (2008).

[25] H. Song and U. W. Heinz, Phys. Lett. B **658**, 279 (2008).

[26] H. Song and U. W. Heinz, Phys. Rev. C **77**, 064901 (2008).

[27] M. Luzum and P. Romatschke, Phys. Rev. C **78**, 034915 (2008); **79**, 039903(E) (2009).

[28] H. Song and U. W. Heinz, Phys. Rev. C **78**, 024902 (2008).

[29] M. Luzum and P. Romatschke, Phys. Rev. Lett. **103**, 262302 (2009).

[30] U. W. Heinz, J. S. Moreland, and H. Song, Phys. Rev. C **80**, 061901 (2009).

[31] C. Shen, U. Heinz, P. Huovinen, and H. Song, Phys. Rev. C **82**, 054904 (2010).

[32] H. Song, S. A. Bass, U. W. Heinz, T. Hirano, and C. Shen, Phys. Rev. Lett. **106**, 192301 (2011).

[33] H. Song, S. A. Bass, and U. Heinz, Phys. Rev. C **83**, 024912 (2011).

[34] H. Niemi, G. S. Denicol, P. Huovinen, E. Molnar, and D. H. Rischke, Phys. Rev. Lett. **106**, 212302 (2011).

[35] H. Song, S. A. Bass, U. W. Heinz, T. Hirano, and C. Shen, Phys. Rev. C **83**, 054910 (2011).

[36] H. Song, S. A. Bass, and U. W. Heinz, Phys. Rev. C **83**, 054912 (2011).

[37] B. H. Alver, C. Gombeaud, M. Luzum, and J.-Y. Ollitrault, Phys. Rev. C **82**, 034913 (2010).

[38] P. Staig and E. Shuryak, Phys. Rev. C **84**, 044912 (2011).

[39] R. J. Glauber, in *Lectures in Theoretical Physics*, edited by W. E. Brittin *et al.* (Interscience Publishers, New York, 1959), Vol. I, p. 315.

[40] P. F. Kolb, U. W. Heinz, P. Huovinen, K. J. Eskola, and K. Tuominen, Nucl. Phys. A **696**, 197 (2001).

[41] B. Alver, M. Baker, C. Loizides, and P. Steinberg, arXiv:0805.4411 [nucl-ex].

[42] B. Alver, B. B. Back, M. D. Baker, M. Ballintijn, D. S. Barton, R. R. Betts, R. Bindel, W. Busza *et al.*, Phys. Rev. C **77**, 014906 (2008).

[43] T. Hirano and Y. Nara, Phys. Rev. C **79**, 064904 (2009).

[44] H. Pi, Comput. Phys. Commun. **71**, 173 (1992).

[45] X.-N. Wang, Phys. Rev. D **43**, 104 (1991).

[46] R. J. Glauber and G. Matthiae, Nucl. Phys. B **21**, 135 (1970).

[47] M. Alvioli, H.-J. Drescher, and M. Strikman, Phys. Lett. B **680**, 225 (2009).

[48] M. Alvioli and M. Strikman, Phys. Rev. C **83**, 044905 (2011).

[49] M. Alvioli, C. Ciofi degli Atti, I. Marchino, V. Palli, and H. Morita, Phys. Rev. C **78**, 031601 (2008).

[50] M. Alvioli, C. Ciofi degli Atti, B. Z. Kopeliovich, I. K. Potashnikova, and I. Schmidt, Phys. Rev. C **81**, 025204 (2010).

[51] C. Ciofi degli Atti, B. Z. Kopeliovich, C. B. Mezzetti, I. K. Potashnikova, and I. Schmidt, Phys. Rev. C **84**, 025205 (2011).

[52] M. Alvioli, C. Ciofi degli Atti, and H. Morita, Phys. Rev. C **72**, 054310 (2005).

[53] M. Alvioli, C. Ciofi degli Atti, and H. Morita, Phys. Rev. Lett. **100**, 162503 (2008).

[54] A. Tang *et al.*, Phys. Rev. Lett. **90**, 042301 (2003).

[55] R. Shneor *et al.* (Jefferson Lab Hall A. Collaboration), Phys. Rev. Lett. **99**, 072501 (2007).

[56] R. Subedi *et al.*, Science **320**, 1476 (2008).

[57] W. Broniowski and M. Rybczynski, Phys. Rev. C **81**, 064909 (2010).

[58] M. Alvioli, C. Ciofi degli Atti, L. P. Kaptari, C. B. Mezzetti, H. Morita, and S. Scopetta, Phys. Rev. C **85**, 021001(R) (2012).

[59] H. Feldmeier, W. Horiuchi, T. Neff, and Y. Suzuki, Phys. Rev. C **84**, 054003 (2011).

[60] M. Vanhalst, W. Cosyn, and J. Ryckebusch, Phys. Rev. C **84**, 031302 (2011).

[61] B. Blattel, G. Baym, L. L. Frankfurt, H. Heiselberg, and M. Strikman, Phys. Rev. D **47**, 2761 (1993).

[62] G. Baym, B. Blattel, L. L. Frankfurt, H. Heiselberg, and M. Strikman, Phys. Rev. C **52**, 1604 (1995).

[63] N. Borghini and J.-Y. Ollitrault, Phys. Lett. B **642**, 227 (2006).

[64] J.-Y. Ollitrault, A. M. Poskanzer, and S. A. Voloshin, Phys. Rev. C **80**, 014904 (2009).

[65] M. Rybczynski and W. Broniowski, Phys. Rev. C **84**, 064913 (2011).